Doping-enhanced robustness of anomaly-related magnetoresistance in $WTe_{2\pm\alpha}$ flakes

Jianchao Meng(孟建超)[1,2], Xinxiang Chen(陈鑫祥)[1], Tingna Shao(邵婷娜)[1], Mingrui Liu(刘明睿)[3], Weimin Jiang(姜伟民)[1], Zitao Zhang(张子涛)[1], Changmin Xiong(熊昌民)[1], Ruifen Dou(窦瑞芬)[1,†], and Jiacai Nie(聂家财)[1,‡]

[1] *Department of Physics, Beijing Normal University, Beijing* 100875, *China*
[2] *College of Science, Inner Mongolia University of Technology, Hohhot* 010051, *China*
[3] *State Key Laboratory of Luminescence and Applications, Changchun Institute of Optics, Fine Mechanics and Physics, Chinese Academy of Sciences, Changchun* 130033, *China*

(Received 17 September 2022; revised manuscript received 12 December 2022; accepted manuscript online 18 January 2023)

We study systematically the negative magnetoresistance (*MR*) effect in $WTe_{2\pm\alpha}$ flakes with different thicknesses and doping concentrations. The negative *MR* is sensitive to the relative orientation between electrical-/magnetic-field and crystallographic orientation of $WTe_{2\pm\alpha}$. The analysis proves that the negative *MR* originates from chiral anomaly and is anisotropic. Maximum entropy mobility spectrum is used to analyze the electron and hole concentrations in the flake samples. It is found that the negative *MR* observed in $WTe_{2\pm\alpha}$ flakes with low doping concentration is small, and the high doping concentration is large. The doping-induced disorder obviously inhibits the positive *MR*, so the negative *MR* can be more easily observed. In a word, we introduce disorder to suppress positive *MR* by doping, and successfully obtain the negative *MR* in $WTe_{2\pm\alpha}$ flakes with different thicknesses and doping concentrations, which indicates that the chiral anomaly effect in WTe_2 is robust.

Keywords: Weyl semimetal, $WTe_{2\pm\alpha}$ flakes, doping, chiral anomaly, robustness

PACS: 75.47.–m, 61.46.–w, 61.72.–y **DOI:** 10.1088/1674-1056/acb423

1. Introduction

The discovery of Dirac/Weyl semimetals has triggered experimental exploration of novel quantum phenomena. Theoretically, the Weyl fermion with well-defined chirality will spontaneously transform into the opposite chirality when a magnetic field (B) is applied parallel to an electric field (E), and an additional current will be generated in this process, so that negative magnetoresistance (*MR*, $MR = \frac{\rho(B)-\rho(0)}{\rho(0)} \times 100\%$) can be observed in the transport. This state of chiral charge imbalance is called chiral anomaly. Since negative *MR* is related to the pumping of chiral charge between the two branches, it is considered as an important feature of the existence of chiral anomaly.[1–6] Thus far, negative *MR* phenomenon has been observed in various topological semimetals, including Na_3Bi,[7,8] Cd_3As_2,[9,10] $ZrTe_5$,[11] TaAs,[12] WTe_2.[13–16] Due to the difference of point-like Fermi surface (type-I) and tilted Weyl cones (type-II), the transport properties of these two types of Dirac/Weyl semimetals are also significantly different.[17,18] For example, the negative *MR* caused by chiral anomaly can be observed in type-I Dirac/Weyl semimetals in any direction,[19] while the chiral anomaly in the type-II Dirac/Weyl semimetals shows anisotropic, and negative *MR* can be observed only in a specific direction in the reciprocal space.[17]

Transitional metal chalcogenide WTe_2 is the first candidate for type-II Weyl semimetal, and there are many experiments about the negative *MR* phenomenon related to the chiral anomaly.[13,15,16] However, due to the large positive *MR*, the negative *MR* was only reported in specific samples with a finite thickness (7 nm–15 nm)[13] or in bulk with specific electron doping (such as $WTe_{1.98}$ crystals).[15] Recently, Hiroaki Ishizuka and Naoto nagaosa[20] theoretically inferred that even if the Fermi level is far away from the Weyl point in the semiclassical limit, the contribution of chiral anomaly to longitudinal *MR* will not disappear. Using the Boltzmann theory, the electric current associated with chiral anomaly can be written in the following form:

$$\boldsymbol{J}_{\rm ano} = \tau q^4 \sum_{\alpha} \int \frac{{\rm d}^3 k}{(2\pi)^3} \boldsymbol{W}_{k\alpha} [\boldsymbol{E} \cdot \boldsymbol{W}_{k\alpha}] \delta(\varepsilon_{k\alpha} - \mu), \quad (1)$$

where τ is the relaxation time, q is the charge of the particle, $\boldsymbol{E}$ is the electric field, μ is the chemical potential, α, k, and $\varepsilon_{k\alpha}$ are band, momentum, and the energy of the state, respectively; $\boldsymbol{W}_{k\alpha} \equiv \boldsymbol{b}_{k\alpha} \times (\boldsymbol{v}_{k\alpha} \times \boldsymbol{B})$ ($\boldsymbol{b}_{k\alpha}$ and $\boldsymbol{v}_{k\alpha}$ are the Berry curvature and group velocity). When a magnetic field $\boldsymbol{B}$ is applied along the unit vector $\boldsymbol{e}_E$, the $\boldsymbol{J}_{\rm ano}$ in the unit vector direction is

$$\boldsymbol{J}_{\rm ano} \cdot \boldsymbol{e}_E = \tau q^4 E \sum_{\alpha} \int \frac{{\rm d}^3 k}{(2\pi)^3} (\boldsymbol{e}_E \cdot \boldsymbol{W}_{k\alpha})^2 \delta(\varepsilon_{k\alpha} - \mu), \quad (2)$$

†Corresponding author. E-mail: rfdou@bnu.edu.cn
‡Corresponding author. E-mail: jcnie@bnu.edu.cn

© 2023 Chinese Physical Society and IOP Publishing Ltd

where $E = |\boldsymbol{E}|$. Since the berry curvature induced by the Weyl nodes is non-zero, $\boldsymbol{b}_{k\alpha} \neq 0$ (*i.e.*, $\boldsymbol{W}_{k\alpha} \neq 0$), the induced electric current in the direction of the electric field always contributes to the conductivity, *i.e.*, the longitudinal *MR* is always negative. The above theoretical derivation shows that even if we move the Weyl point away from the Fermi level by doping or other means, the contribution of different Weyl nodes to the conductivity still exists, and the negative *MR* phenomenon can be observed in the transport. If the large positive *MR* is suppressed by doping, the negative *MR* should not be observed only in flakes with finite thickness or specific doping concentration.[20]

In this paper, positive *MR* is suppressed by doping, negative *MR* was observed in the $WTe_{2\pm\alpha}$ flakes with different thicknesses and doping concentrations. It is found that negative *MR* induced by chiral anomaly can only be observed in *b*-axis direction in all flakes, while the positive *MR* is shown in other directions, proving that the chiral anomaly in WTe_2 is anisotropic. The observation of negative *MR* in $WTe_{2\pm\alpha}$ flakes with different thicknesses and doping concentrations shows that the chiral anomaly effect in WTe_2 is robust.

2. Experiments

$WTe_{2\pm\alpha}$ flakes with different thicknesses and doping concentrations were exfoliated from the single crystal $WTe_{2\pm\alpha}$ (purchased from Nanjing MKNANO Tech. Co., Ltd.). X-ray diffraction (XRD, Shimadzu XRD-600, Japan) measurements (Fig. 1(a)) shows that the single crystal has a stable T_d phase. The chemical composition of $WTe_{2\pm\alpha}$ flakes was confirmed by energy dispersive x-ray spectroscopy (EDS) analysis. As shown in Fig. 1(b) and the inset, we performed EDS analysis on the three micro-regions in each sample, and selected flakes with uniform component distribution as experimental flake samples. The flakes used in the experiment are $WTe_{1.42}$ (210 nm), $WTe_{1.61}$ (200 nm), $WTe_{1.85}$ (190 nm), $WTe_{1.93}$ (150 nm), and $WTe_{2.18}$ (90 nm), respectively. Since chiral anomaly in $WTe_{2\pm\alpha}$ flakes may be anisotropic, we need to determine the crystal orientation of the flakes before preparing the electrodes. Here, we use the method of polarized Raman spectra, which judges the crystal orientation through the periodic change of the Raman spectrum with the polarization angle. Figure 1(c) shows the non-polarized Raman spectra of a typical single crystal sample, and figure 1(d) is the polarized Raman spectra of the flake (the value of P3 peak and P5 peak changes periodically with the polarization angle). According to the research results of Kong *et al.*,[21] the intensity of peak P3 is the weakest in the direction of *b* axis, and the intensity of the P5 peak is the strongest; while in the *a*-axis direction, it is just the opposite. In this way, we can use the intensity difference between the P3 and P5 peaks to determine the crystal orientation in $WTe_{2\pm\alpha}$. The red arrow marked in Fig. 1(b) is the *b*-axis direction obtained by analyzing the Raman measurement results.

After determining the crystal orientation, a double-cross-pattern electrode was fabricated, as shown in Fig. 1(b), so that we can simultaneously study whether there is negative *MR* effect in the *a*-axis, *b*-axis, and 45° directions in the same sample. The transport properties were measured by a physical property measurement system (9 T PPMS, Quantum Design) from 2 K to 300 K in a magnetic field of up to 9 T.

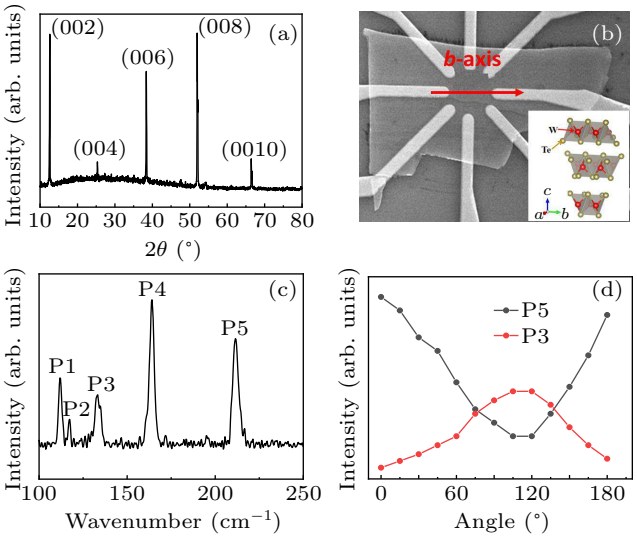


Fig. 1. Characterization of $WTe_{2\pm\alpha}$: (a) XRD pattern of the crystal structure, (b) scanning electron microscopy (SEM) image of the $WTe_{2\pm\alpha}$ flake with Cr/Au (5/100 nm) electrodes. Scale bar: 6 μm. The inset shows the crystal structure of WTe_2. (c) The non-polarized Raman spectra of a typical single crystal sample. (d) The polarized Raman spectra of the flake.

3. Results and discussion

We study the negative *MR* effect of five $WTe_{2\pm\alpha}$ flakes with different thicknesses and doping concentrations. It was found that the five flake samples all show negative *MR* effect in the *b*-axis direction when the electric field parallel to the magnetic field, which is due to the chiral anomaly and is well consistent with the previous observation.[13,16] Figure 2(a) shows the negative *MR* of five flake samples at 2 K, the inset shows a schematic of the measurement configuration. It can be seen that the flakes with the highest electron doping concentration, that is, the $WTe_{1.42}$ flake, has the largest negative *MR*, which can reach −15.86%. As the doping concentration decreases, the negative *MR* gradually decreases, and the negative *MR* in the $WTe_{1.93}$ flake is −4.96%. The negative *MR* can also be observed in the hole-doped $WTe_{2.18}$ flake. Figure 2(b) shows that negative *MR* of $WTe_{1.93}$ flake gradually decreases with the increase of temperature when the electric field and magnetic field remain parallel, and can still be observed at 70 K. It is can be seen that the positive *MR* appears at low temperature and small magnetic field in most of the flake samples

($WTe_{1.61}$, $WTe_{1.85}$, $WTe_{1.93}$, and $WTe_{2.18}$), implying a signal of weak anti-localization. In the $WTe_{1.42}$ flake, no weak anti-localization phenomenon was observed, we cannot rule out that weak anti-localization can be observed at lower temperatures as this phenomenon will disappears with the increase of temperature. Figure 2(c) presents the longitudinal *MR* of the $WTe_{1.93}$ flake along the *a* axis, *b* axis, and 45°, the electric field and magnetic field are also strictly parallel along these three directions during measurement. Negative *MR* phenomenon is observed only along the *b* axis, but not along the *a* axis. In the direction of 45°, the longitudinal *MR* tends to decrease obviously under high magnetic field, and there may be a competition between negative *MR* and positive *MR*.

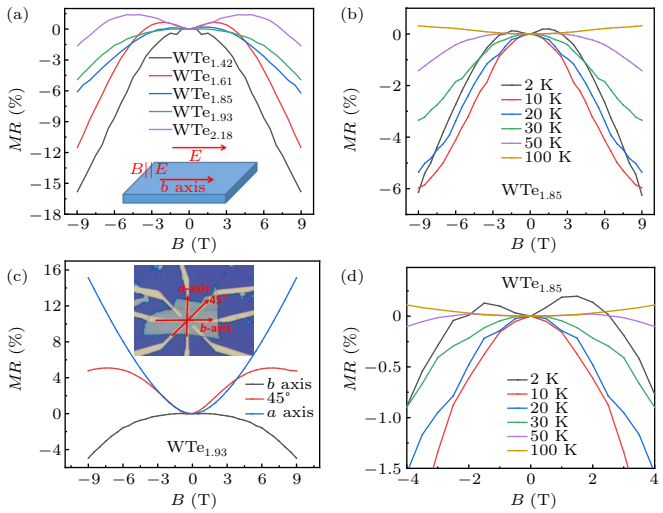


Fig. 2. Negative *MR* in $WTe_{2\pm\alpha}$, the electric field and magnetic field remain parallel during the measurements. (a) The longitudinal negative *MR* in the *b*-axis direction of five flake samples with different doping concentrations ($WTe_{1.42}$, $WTe_{1.61}$, $WTe_{1.85}$, $WTe_{1.93}$, and $WTe_{2.18}$) at 2 K. The inset shows a schematic diagram of the measurement configuration. (b) Temperature dependence of the negative *MR* in $WTe_{1.93}$ flake. (c) Longitudinal *MR* along the *a*-axis, *b*-axis, and 45° directions in the $WTe_{1.93}$ flake. The inset shows the illustration of the measurement direction. (d) An enlarged view of negative *MR* in panel (b) near zero magnetic field.

When analyzing negative *MR*, we first need to exclude other sources other than chiral anomaly, such as current jetting effect, magnetic effect, and the weak localization effect.[22–27] Since WTe_2 is non-magnetic, the magnetic effect can be eliminated first. The weak localization effect also causes a negative *MR* when the electric field is perpendicular to the in-plane magnetic field, thus the negative *MR* is not caused by the weak localization effect.[27] Current jetting effect generally occurs in materials with high mobility (*e.g.*, TaP),[22] while our flake materials have low mobility and weak current jetting effect, and will not lead to negative *MR* effect. Based on the above analysis, we believe that the negative *MR* effect observed in the $WTe_{2\pm\alpha}$ flakes is caused by the chiral anomaly.

Next we measured the dependence of the negative *MR* along the *b*-axis on the angle (θ) between the electric field and the magnetic field. Figure 3(a) shows the measurement results of the $WTe_{1.85}$ flake, the negative *MR* decreases rapidly with increase of θ and almost disappears when $\theta = 2°$. The conductivity induced by the chiral anomaly can be analyzed by semi-classical equations[28]

$$\sigma(B) = \left(1 + C_W B^2\right) \cdot \sigma_{WAL} + \sigma_N, \tag{3}$$

$$\sigma_{WAL} = \sigma_0 + a\sqrt{B}, \tag{4}$$

where C_W is a positive parameter that originates from the chiral anomaly when the electric field parallel to the magnetic field, σ_0 is conductivity under zero magnetic field, σ_{WAL} is a parameter from the anti-localization effect and σ_N is from Fermi surface. When 0 T $< B <$ 4 T, equation (3) is used to fit the negative *MR* curves at 2 K. We can see that the experimental data can be well fitted (Fig. 3(b)). The inset shows the parameter C_W extracted from the fitting data, C_W is 0.022 when $\theta = 0°$, and close to 0 when $\theta = 2°$. C_W is sensitive to the change of θ, which further confirms that the negative *MR* in $WTe_{2\pm\alpha}$ flakes is induced by the chiral anomaly.

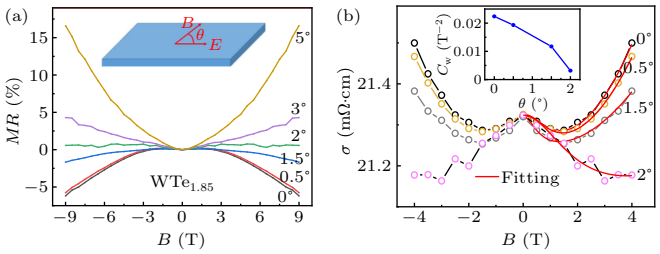


Fig. 3. (a) The dependence of the negative *MR* on the angle θ between the electric field and the magnetic field in the $WTe_{1.85}$ flake. The inset is a schematic diagram of the measurement configuration. (b) The curves of conductivity with magnetic field at different θ and the fitting curves using Eq. (3). The inset shows the θ dependence of C_W, obtained from the fitting data.

The above results show that the doping concentration of the flakes has a great influence on the negative *MR*. Doping has an important effect in this experiment, which can produce disorder in the flake samples, thereby suppressing the larger positive *MR* and making the negative *MR* effect easier to observe. Here, we use the maximum entropy mobility spectrum (MEMS)[29,30] to analyze the electron and hole concentrations (n_e, n_h) in the $WTe_{2\pm\alpha}$ flakes. MEMS introduces the principle of maximum entropy[31] into the mobility (μ) spectrum, and transforms the magnetic field dependence of conductivity tensor (σ_{xx}, σ_{yx}) into the mobility dependence of the electrical conductivity density function ($s(\mu)$) (related to the electrical conductivity tensor). Figure 4(a) shows the normalized MEMS at 2 K for the five flake samples. The results of MEMS analysis are summarized in Table 1. It is can be seen that the doping concentration in $WTe_{1.42}$ flake is the largest, the n_e/n_h ratio is 1.22. The n_e/n_h ratio of the $WTe_{1.93}$ flake, which is close to the stoichiometric ratio, is 1.06. The n_e/n_h ratio in the hole-doped $WTe_{2.18}$ flake is 0.80. Lv *et al.*[15] calculated that the position of Weyl point in the stoichiometric WTe_2 is about

60 meV above the Fermi surface, slight electron doping can adjust the position of the Weyl point to be close to the Fermi level, which is more conducive to the observation of negative *MR*. Thus, we can observe negative *MR* in low electron doped flake samples ($WTe_{1.84}$, $WTe_{1.93}$). For the flake samples with high doping concentration ($WTe_{1.42}$, $WTe_{1.61}$), the Weyl point is relatively far from the Fermi level, a negative *MR* can still be observed, which may be related to the suppression of positive *MR* by doping.

Table 1. Thickness, negative *MR*, negative *MR* per unit thickness (nm), and n_e/n_h ratio of five $WTe_{2\pm\alpha}$ flake samples with different thicknesses and doping concentrations (2 K).

Samples	Thickness (nm)	Negative *MR*	Negative *MR* per unit thickness (nm)	n_e/n_h ratio
$WTe_{1.42}$	210	−15.86%	−0.076%	1.22
$WTe_{1.61}$	200	−11.50%	−0.058%	1.12
$WTe_{1.85}$	190	−6.10%	−0.032%	1.09
$WTe_{1.93}$	150	−4.96%	−0.033%	1.06
$WTe_{2.18}$	90	−1.65%	−0.018%	0.80

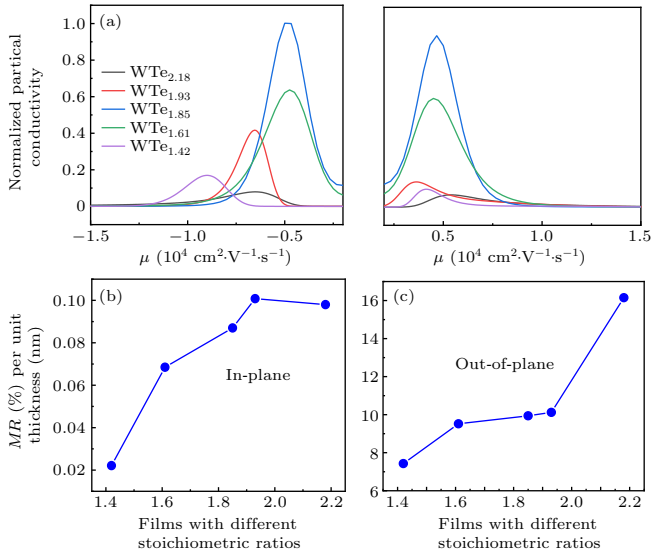


Fig. 4. (a) Normalized MEMS at 2 K of the five flake samples. The peaks at negative and positive mobility represent the electron and hole, respectively. (b) Positive *MR* per unit thickness (in unit nm) of the five flake samples under 9 T at 2 K when the electric field perpendicular to the in-plane magnetic field. (c) Positive *MR* per unit thickness (in unit nm) of the five flake samples under 9 T at 2 K when the electric field perpendicular to the out-of-plane magnetic field.

Then, we discuss the suppression effect of doping on the large positive *MR* in $WTe_{2\pm\alpha}$. Since the large positive *MR* can conceal the signal of negative *MR* when the electrical field is not rigorously parallel to magnetic field, and the thickness of the flake samples is positively correlated with the *MR*,[32] therefore, we calculated the positive *MR* per unit thickness (in unit nm) to exclude the effect of flake thickness.

In the experiment, it is difficult to separate the positive *MR* from the negative *MR* direction when the electric field and magnetic field are parallel, so we measured the positive *MR* in other configurations. Figure 4(b) shows the positive *MR* per unit thickness of the five flake samples under 9 T at 2 K, when the electric field is perpendicular to the in-plane magnetic field. When the electric field is perpendicular to the out-of-plane magnetic field, the positive *MR* effect is the strongest.[33] Figure 4(c) shows the positive *MR* per unit thickness under 9 T at 2 K when the electric field is perpendicular to the out-of-plane magnetic field. We can see that the positive *MR* of the flakes with higher doping concentration ($WTe_{1.42}$, $WTe_{1.61}$) is significantly suppressed, so the observed negative *MR* is relatively large. While the positive *MR* is less inhibited in the flakes with lower doping concentration ($WTe_{1.84}$, $WTe_{1.93}$, $WTe_{2.18}$), and the negative *MR* is relatively low. According to the previous studies,[30,34] samples with higher doping concentration in WTe_2 introduce more disorder, while the sample purity has a great influence on the large positive *MR*. Therefore, positive *MR* can be suppressed and negative *MR* can be observed more easily for flakes with more disorder. For the hole-doped flake ($WTe_{2.18}$), the Weyl point is relatively far from the Fermi level, but the disorder caused by doping also inhibits the positive *MR*, so a small negative *MR* can also be observed.

The negative *MR* can be observed in flakes with various doping concentrations, which can be attributed to two reasons. First, the chiral anomaly in Weyl semimetal is robust, that is, when the Weyl point is far away from the Fermi level, the negative *MR* induced by the chiral anomaly can still be observed in transport, which is consistent with the theoretical prediction mentioned above. Second, the large and positive *MR* is considered to be related to electron–hole compensation in WTe_2, Te or W vacancies may act as disorder and suppress the charge compensation in the $WTe_{2\pm\alpha}$ film, so it is easier to measure negative *MR* effect for flakes with more doping. We observed the negative *MR* in $WTe_{2\pm\alpha}$ flakes with different thicknesses and doping concentrations, which indicates that the chiral anomaly effect in WTe_2 is robust.

4. Conclusion

We observed the negative *MR* in five $WTe_{2\pm\alpha}$ flakes with different thicknesses and doping concentrations, and found that the negative *MR* was sensitive to the angle between the electric field and magnetic field, and also the crystal orientation of the flake samples. The results of MEMS analysis show that the negative *MR* of the flakes with high doping concentration is larger than that of low doping concentration flakes. We successfully introduced disorder into the flake to suppress the positive *MR*. In a word, negative *MR* is observed in $WTe_{2\pm\alpha}$ flakes with different thicknesses and doping concentrations, indicating that there is a robust chiral anomaly effect in WTe_2, which may provide a prospect for the future use of chiral fermions in electronic applications.

Acknowledgments

Project supported by the National Natural Science Foundation of China (Grant Nos. 92065110, 11674031, 11974048, and 12074334) and the National Basic Research Program of China (Grant Nos. 2014CB920903 and 2013CB921701).

References

[1] Son D and Spivak B Z 2013 *Phys. Rev. B* **88** 104412
[2] Wan X, Turner A M, Vishwanath A and Savrasov S Y 2011 *Phys. Rev. B* **83** 205101
[3] Xiong J, Kushwaha S K, Liang T, Krizan J W, Hirschberger M, Wang W, Cava R J and Ong N P 2015 *Science* **350** 413
[4] Hirschberger M, Kushwaha S, Wang Z, Gibson Q, Liang S, Belvin C A, Bernevig B A, Cava R J and Ong N P 2016 *Nat. Mater.* **15** 1161
[5] Zhang C, Xu S, Belopolski I, Yuan Z, Lin Z, Tong B, Bian G, Alidoust N and Lee C 2016 *Nat. Commun.* **7** 1
[6] Niemann A C, Gooth J, Shu C W, Svenja B, Philip S, Ruben H, Bernd R, Chandra S, Vicky S, Marcus S, Claudia F, Yan B and Kornelius N 2017 *Sci. Rep.* **7** 43394
[7] Liu Z, Zhou B, Zhang Y, Wang Z, Weng H, Prabhakaran D, Mo S, Shen Z, Fang, Z, Dai X, Hussain Z and Chen Y 2018 *Science* **12** 6700
[8] Liang S, Lin J, Kushwaha S, Xing J, Ni N, Cava R J and Ong N P 2018 *Phys. Rev. X* **8** 031002
[9] He L, Hong X, Dong J, Pan J, Zhang Z, Zhang J and Li S 2014 *Phys. Rev. Lett.* **113** 246402
[10] Jeon S, Zhou B, Gyenis A, Feldman B, Kimchi I, Potter A, Gibson Q, Cava R J, Vishwanath A and Yazdani A 2014 *Nat. Mater.* **13** 851
[11] Li Q, Kharzeev D E, Zhang C, Huang Y, Pletikosic I, Fedorov A V, Zhong R D, Schneeloch J A, Gu G and Valla T 2016 *Nat. Phys.* **12** 550
[12] Huang X, Zhao L, Long Y, Wang P, Chen D, Yang Z, Liang H, Xue M, Weng H, Fang Z, Dai X and Chen G 2015 *Phys. Rev. X* **5** 031023
[13] Wang Y, Liu E, Liu H, Pan Y, Zhang L, Zeng J, Fu Y, Wang M, Xu K, Huang Z, Wang Z, Lu H, Xing D, Wang B, Wan X and Miao F 2016 *Nat. Commun.* **7** 13142
[14] Zhang E, Chen R, Huang C, Yu J, Zhang K, Wang W, Liu S, Ling J, Wan X, Lu H and Xiu F 2017 *Nano Lett.* **17** 878
[15] Lv Y, Li X, Zhang B, Deng W, Yao S, Chen Y, Zhou J, Zhang S, Lu M, Zhang L, Tian M, Sheng L and Chen Y 2017 *Phys. Rev. Lett.* **118** 096603
[16] Li P, Wen Y, He X, Zhang Q, Xia C, Yu Z, Yang S, Zhu Z, Alshareef H and Zhang X 2017 *Nat. Commun.* **8** 1
[17] Soluyanov A A, Gresch D, Wang Z, Wu Q, Troyer M, Dai X and Bernevig B 2015 *Nature* **527** 495
[18] Zhang M, Yang Z and Wang G 2018 *J. Phys. Chem. C* **122** 3533
[19] Nielsen H B and Ninomiya M 1981 *Nucl. Phys. B* **185** 20
[20] Ishizuka H and Nagaosa N 2019 *Phys. Rev. B* **99** 115205
[21] Kong W, Wu S, Richard P, Lian C, Wang J, Yang C, Shi Y and Ding H 2015 *Appl. Phys. Lett.* **106** 081906
[22] Arnold F, Shekhar C, Wu S, Sun Y, Dos Reis R D, Kumar N, Naumann M, Ajeesh M O, Schmidt M, Grushin A G, Bardarson J H, Baenitz M, Sokolov D, Borrmann H, Nicklas M, Felser C, Hassinger E and Yan B 2016 *Nat. Commun.* **7** 11615
[23] Schumann T, Goyal M and Kealhofer D A 2017 *Phys. Rev. B* **95** 241113
[24] Dos Reis R, Ajeesh M, Kumar N, Arnold F, Shekhar C, Naumann M, Schmidt M, Nicklas M and Hassinger E 2016 *New J. Phys.* **18** 085006
[25] Li Y, Wang Z, Li P, Yang X, Shen Z, Sheng F, Li X, Lu Y, Zheng Y and Xu Z 2017 *Front. Phys.* **12** 1
[26] Ritchie L, Xiao G, Ji Y, Chen T, Chien C, Zhang M, Chen J, Liu Z, Wu G and Zhang X 2003 *Phys. Rev. B* **68** 104430
[27] Li Z, Zeng Y, Zhang J, Zhou M and Wu W 2018 *Phys. Rev. B* **98** 165441
[28] Kim H J, Kim K S, Wang J, Sasaki M, Satoh N, Ohnishi A, Kitaura M, Yang M and Li L 2013 *Phys. Rev. Lett.* **111** 246603
[29] Kiatgamolchai S, Myronov M, Mironov O A, Kantser V G, Parker E H and Whall T E 2002 *Phys. Rev. E* **66** 036705
[30] Meng J, Chen X, Liu M, Jiang W, Zhang Z, Ling J, Shao T, Yao C, He L, Dou R, Xiong C and Nie J 2020 *J. Phys.: Condens. Matter.* **32** 355703
[31] Jaynes E T 1957 *Phys. Rev.* **106** 620
[32] Xiang F, Srinivasan A, Du Z, Klochan O, Dou S, Hamilton A R and Wang X 2018 *Phys. Rev. B* **98** 035115
[33] Zhao Y, Liu H, Yan J, An W, Liu J, Zhang X, Wang H, Liu Y, Jiang H, Li Q, Wang Y, Li X, Mandrus D, Xie X, Pan M and Wang J 2015 *Phys. Rev. B* **92** 041104
[34] Ali M N, Schoop L, Xiong J, Flynn S, Gibson Q, Hirschberger M, Ong N P and Cava R J 2015 *Europhys. Lett.* **110** 67002